DFT Study of Catalytic Styrene Oxidation Using a Bis-Semicarbazide Hexaazamacrocyclic Cu Complex I—Preliminary Calculations

Martin Breza *

Posted Date: 26 June 2025

doi: 10.20944/preprints202506.2108.v1

Keywords: B3LYP hybrid functional; broken symmetry treatment; geometry optimization; electronic structure; Cu oxidation state

 doi:10.20944/preprints202506.2108.v1

Article

DFT Study of Catalytic Styrene Oxidation Using a Bis-Semicarbazide Hexaazamacrocyclic Cu Complex I—Preliminary Calculations

Martin Breza

Department of Physical Chemistry, Slovak Technical University, Radlinskeho 9, SK-81237 Bratislava, Slovakia; martin.breza@stuba.sk

Abstract

The catalytic styrene Ph-CH=CH_2 oxidation is assumed to be a simple reaction procedure, but its details require further systematic research. Using quantum-chemical treatment, relevant intermediates in various charge and spin states of three reaction pathways of styrene oxidation by hydroperoxyl were investigated. The reaction pathway A without any catalyst most probably proceeds by non-radical mechanism and ^{1}[Ph-CH(O)-CH_2OH]$^-$ is formed. The alternative formation of epoxide is energetically less advantageous. The reaction pathways B and C are based on the [CuL]$^-$ catalyst where H_2L = *trans*-2,9-dibutyl-7,14-dimethyl-5,12-di(4-methoxyphenyl)-1,2,4,8,9,11-hexaazacyclotetradeca-7,14-diene-3,10-dione. Within reaction pathway B the neutral hydroperoxyl radical is bonded to Cu to form ^{2}[CuL(OOH)]$^-$. Subsequent addition of neutral styrene results in ^{2}{[CuL(OH)](Ph-CH_2-CHO)}$^-$ formation. The reaction pathway C starts with the initial non-radical formation of the π-complex ^{1}[CuL(Ph-CH=CH_2)]$^-$ which is problematic due to its endothermic character. Subsequent addition of a hydroperoxyl radical leads to ^{2}{CuL[Ph-CH(OOH)-CH_2]}$^-$. Its oxidation leads to the separation of Ph-CH(OOH)-CH_2.

Keywords: B3LYP hybrid functional; broken symmetry treatment; geometry optimization; electronic structure; Cu oxidation state

1. Introduction

The catalytic oxidation of styrene is an environmentally friendly path for the production of benzaldehyde, which is an important intermediate for the production of many fine compounds and commodity chemicals [1]. Various catalysts differ in the conversion and selectivity of benzaldehyde, styrene epoxide, phenylacetaldehyde, 1-phenylethane-1,2-diol, benzoic acid, phenylacetaldehyde and other oxidation products. The development of sustainable and effective catalytic systems for the production of benzaldehyde using green oxidants, such as hydrogen peroxide, is highly significant. For the rational design of efficient catalysts, we must know the corresponding reaction mechanisms. Redox-active ligands can contribute to it by storing and providing electrons, modifying the Lewis acidity of the metal, and assisting the formation/breaking of substrate bonding.

The catalytic styrene oxidation is assumed to be a simple reaction procedure, but its details require further systematic research. Knowledge of its important details is crucial for the development of new catalytic systems. Despite intense studies of the catalyzed oxidation of alkenes with hydrogen peroxide, no generally accepted mechanism of these reactions is known.

The Wacker process [2] is an industrial homogeneous catalytic oxidation of ethylene to acetaldehyde in the presence of $PdCl_2$ and $CuCl_2$ that was considered to be well understood. Its mechanism is based on an active intermediate [$PdCl_2$(C_2H_4)(H_2O)], with π-bonded ethylene to Pd(II) central atom.

 doi:10.20944/preprints202506.2108.v1

However, other catalytic studies using transition metal complexes with multidentate ligands suppose that the intermediate M-O-O-H (M is the metal center) is formed and the O-O bond is activated so that the alkene can react with it [3–12]

In our previous study [13], the CuL complex (Figure 1) with *trans*-2,9-dibutyl-7,14-dimethyl-5,12-di(4-methoxyphenyl)-1,2,4,8,9,11-hexaazacyclotetradeca-7,14-diene-3,10-dione (H_2L), a 14-membered bis-semicarbazide hexaazamacrocycle (see Figure S1 in Supplementary Information), was synthesized and characterized by analytical and spectroscopic techniques (IR, UV−vis, ^1H and ^{13}C NMR, ESI mass spectrometry, single-crystal X-ray diffraction, and spectroelectrochemistry). This complex selectively catalyzes the microwave-assisted oxidation of neat styrene to benzaldehyde using hydrogen peroxide (30% aqueous solution) as the oxidizing agent, under low microwave irradiation (25 W) and in the absence of any added solvent. Under optimized conditions (40 min of irradiation at 80 °C), the catalytic system provided benzaldehyde in a yield of up to 81% (turnover frequency up to 2.4×10^3 h 1) as the only product. The CuL catalyst can be very simply separated by cooling to room temperature.

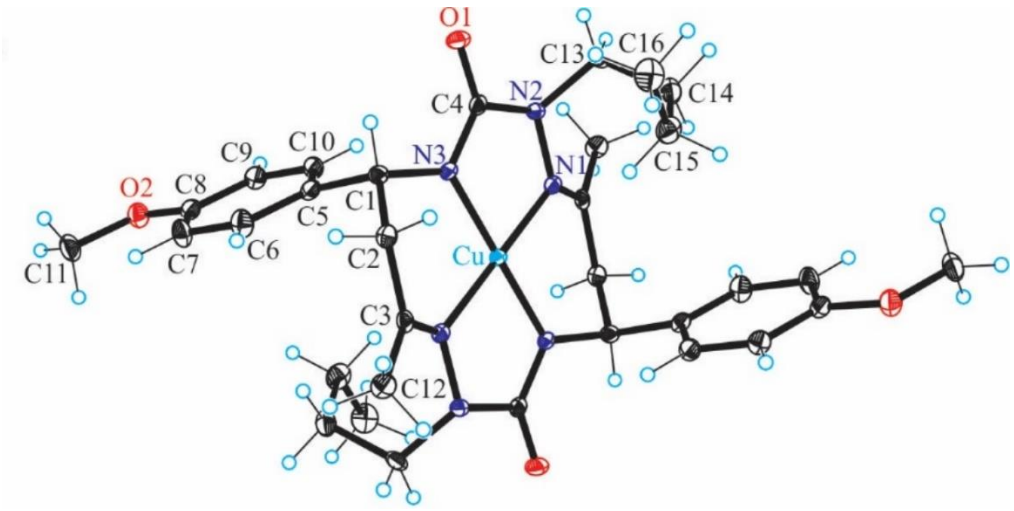

Figure 1. X-ray structure of CuL with atom-labeling scheme and thermal ellipsoids drawn at 50% probability level [13].

In [13] we proposed a free radical mechanism for the catalytic oxidation of styrene. It should be initiated by the Cu-assisted formation of the hydroxyl or hydroperoxyl radicals.

Now we plan to investigate possible mechanisms of styrene oxidation by hydrogen peroxide under CuL catalysis by quantum-chemical treatment. In this part of our study we will investigate structure, energy, and electron structure of relevant intermediates within three reaction pathways.

i) Reaction pathway A is a simple reaction of neutral styrene Ph-CH=CH_2 with hydroperoxyl $(O\text{-}OH)^q$.
ii) Reaction pathway B starts with the formation of a $[CuL(OOH)]^q$ complex followed by styrene addition.
iii) Reaction pathway C starts with the formation of the π-complex $[CuL(Ph\text{-}CH{=}CH_2)]^q$ and subsequent addition of hydroperoxyl.

All intermediates will be studied in various charge q and spin states to account for the noninnocent character of the ligand L^{2-} and possible Cu(II)/Cu(I) equilibria. The obtained results should enable one to propose a realistic reaction pathway which will be studied in more detail in the next parts of this study.

 doi:10.20944/preprints202506.2108.v1

2. Results and Discussion

2.1. Reaction Pathway A

Selected energy and structure parameters of DFT optimized styrene, hydroperoxyl, and their reaction products in various charge and spin states are presented in Tables 1 and S1 – S3 of Supplementary Information; their pictures are in Figures 2 -3 and S2 – S4 of Supplementary Information. The addition of the O – O_H bond

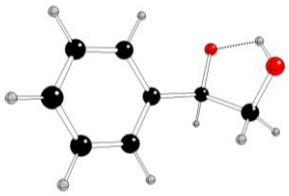

Figure 2. DFT optimized structure of [Ph-C_αH(O)-$C_\beta H_2$OH]$^-$ in singlet spin state (C – black, O – red, H – gray).

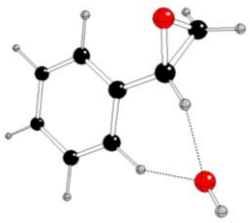

Figure 3. DFT optimized structure of [(Ph-C_αH-C_βH2)(OH)]- in singlet spin state.

\ /

O

(C – black, O – red, H – gray).

Table 1. Relative DFT energies, ΔE_{DFT}, and Gibbs energies at 298 K, ΔG_{298}, of the compounds under study with charges q and spin multiplicities M_s. The energy values are related to the most stable systems (in bold) of the same composition.

	q	M_s	ΔE_{DFT} [kJ/mol]	ΔG_{298} [kJ/mol]
Reaction path A				
$(OOH)^q$	0	2	94.99	97.20
	-1	**1**	**0.00**	**0.00**
	-1	3	67.03	53.90
[Ph-CH(O)-CH_2OH]^q	0	2	251.65	252.31
	-1	**1**	**0.00**	**0.00**
	-1	3	321.52	307.97
[Ph - CH – CH_2(OH)]^q	0	2	379.46	365.86
\ /				
O				
	-1	1	139.13	128.78
	-1	3	277.67	245.69

 doi:10.20944/preprints202506.2108.v1

Reaction path B				
$[CuL]^q$	0	2	127.26	148.50
	-1	**1**	**0.00**	**0.00**
	-1	3	90.95	97.98
	+1	1	748.24	776.49
	+1	3	778.22	799.62
$[CuL(OOH)]^q$	0	1	224.48	232.30
	0	3	224.43	226.92
	-1	**2**	**0.00**	**0.00**
$\{[CuL(OH)](Ph\text{-}CH_2\text{-}CHO)\}^q$	0	1	322.18	341.47
	0	3	323.41	333.39
	-1	**2**	**0.00**	**0.00**
Reaction path C				
$[CuL(Ph\text{-}CH{=}CH_2)]^q$	**-1**	**1**	**0.00**	**0.00**
	-1	3	37.81	20.01
	0	2	85.46	74.80
$\{CuL[Ph\text{-}CH(OOH)\text{-}CH_2]\}^q$	0	1	184.97	182.87
	0	3	197.46	188.30
	-1	**2**	**0.00**	**0.00**

of hydroperoxyl parallel to the C_α - C_β bond of styrene (with C – O distances of about 1.7 – 1.9 Å) leads after geometry optimization to $[Ph\text{-}CH(O)\text{-}CH_2OH]^q$, whereas the analogous perpendicular position leads to epoxides. Independent of the charge and spin states, these epoxides are energetically so high that their formation will not be considered in further studies. According to our results, the most stable structures of $(OOH)^q$ and $[Ph\text{-}CH(O)\text{-}CH_2OH]^q$ correspond to the charge q = -1 in the singlet ground spin state. This finding makes the radical mechanism of styrene oxidation improbable. The O – O_H bond in the $(OOH)^-$ in triplet spin state is split. The hydroxyl group in epoxides is bonded by hydrogen bonding, its charge is negative in $[Ph\text{-}CH(O)\text{-}CH_2OH]^-$ in singlet state, whereas in other systems hydroperoxyl is nearly neutral with one unpaired electron (Tables 2 – 3). The oxygen bond to $C_{\alpha/\beta}$ weakens the C_α – C_β bond in all the systems under study (Table 4).

Table 2. Natural charges of C_α, C_β, O, O_H and H_O atoms in (O-O_H-H_O) and (Ph-C_αH=$C_\beta H_2$) units with charges q and spin multiplicities M_s.

	q	M_s	C_α	C_β	O	O_H	H_O
Reaction path A							
$(OOH)^q$	0	2	-	-	-0.145	-0.305	0.450
	-1	1	-	-	-0.767	-0.630	0.396
	-1	3	-	-	-0.511	-0.890	0.401
$Ph\text{-}CH{=}CH_2$	0	1	-0.191	-0.346	-	-	-
$[Ph\text{-}CH(O)\text{-}CH_2OH]^q$	0	2	0.052	0.012	-0.350	-0.691	0.565
	-1	1	0.106	-0.036	-0.945	-0.795	0.477
	-1	3	-0.025	-0.345	-0.360	-0.763	0.388
$Ph\text{-}CH\text{-}CH_2(OH)]^q$	0	2	0.090	-0.044	-0.586	-0.434	0.416
\ /							
O							

 doi:10.20944/preprints202506.2108.v1

	-1	1	0.042	-0.056	-0.587	-1.319	0.390
	-1	3	-0.025	-0.345	-0.763	-0.360	0.388
Reaction path B							
$[CuL(OOH)]^q$	0	1	-	-	-0.167	-0.317	0.484
	0	3	-	-	-0.167	-0.317	0.484
	-1	2	-	-	-0.614	-0.514	0.437
$\{[CuL(OH)](Ph\text{-}CH_2\text{-}CHO)\}^q$	0	1	-0.488	0.446	-0.566	-0.925	0.433
	0	3	-0.488	0.448	-0.561	-0.856	0.437
	-1	2	-0.491	0.436	-0.584	-1.188	0.424
Reaction path C							
$[CuL(Ph\text{-}CH{=}CH_2)]^q$	-1	1	-0.277	-0.472	-	-	-
	-1	3	-0.240	-0.452	-	-	-
	0	2	-0.192	-0.356	-	-	-
$\{CuL[Ph\text{-}CH(OOH)\text{-}CH_2]\}^q$	0	1	0.019	-0.251	-0.327	-0.452	0.461
	0	3	0.012	-0.228	-0.319	-0.452	0.457
	-1	2	0.081	-0.785	-0.347	-0.454	0.440

Table 3. Natural spin populations at C_α, C_β, O, O_H and H_O atoms in (O-O_H-H_O) and (Ph-C_αH=$C_\beta H_2$) units with charges q and spin multiplicities M_s.

	q	M_s	C_α	C_β	O	O_H	H_O
Reaction path A							
$(OOH)^q$	0	2	-	-	0.742	0.268	-0.010
	-1	1	-	-	0.000	0.000	0.000
	-1	3	-	-	1.479	0.535	-0.014
$Ph\text{-}CH{=}CH_2$	0	1	0.000	0.000	0.000	0.000	0.000
$[Ph\text{-}CH(O)\text{-}CH_2OH]^q$	0	2	-0.029	0.116	0.820	0.033	0.000
	-1	1	0.000	0.000	0.000	0.000	0.000
	-1	3	0.050	0.346	0.862	0.032	0.074
$[Ph - CH - CH_2(OH)]^q$ \ / O	0	2	0.000	0.000	0.001	1.021	-0.023
	-1	1	0.000	0.000	0.000	0.000	0.000
	-1	3	0.568	-0.025	0.211	0.967	-0.018
Reaction path B							
$[CuL(OOH)]^q$	0	1	-	-	0.701	0.310	-0.008
	0	3	-	-	0.702	0.309	-0.008
	-1	2	-	-	0.097	0.007	0.001
$\{[CuL(OH)](Ph\text{-}CH_2\text{-}CHO)\}^q$	0	1	-0.002	-0.004	-0.005	-0.343	0.008
	0	3	0.002	0.004	0.005	0.435	-0.011
	-1	2	0.000	0.000	0.000	0.035	-0.001
Reaction path C							
$[CuL(Ph\text{-}CH{=}CH_2)]^q$	-1	1	0.000	0.000	-	-	-

 doi:10.20944/preprints202506.2108.v1

	-1	3	0.042	0.174	-	-	-
	0	2	0.000	0.000	-	-	-
{CuL[Ph-CH(OOH)-CH_2]}^{q}	0	1	0.035	-0.998	-0.021	-0.006	0.000
	0	3	-0.029	0.982	0.065	0.000	0.000
	-1	2	-0.001	0.254	0.022	-0.001	0.000

Our results indicate that the most probable non-radical styrene oxidation in singlet spin state

$$Ph\text{-}CH{=}CH_2 + (OOH)^- \rightarrow [Ph\text{-}CH(O)\text{-}CH_2OH]^- \quad (1)$$

is highly exotermic (Gibbs reaction energy at normal condition Δ_rG_{298} = -307.84 kJ/mol, compare Table S1 in Supplementary Information).

Table 4. Overlap weighted bond orders between C_α, C_β, O, O_H and H_O atoms in (O-O_H-H_O) and (Ph-C_αH=$C_\beta H_2$) units with charges q and spin multiplicities M_s.

	q	M_s	C_α-C_β	C_α-O	C_α-O_H	C_β-O	C_β-O_H	O-O_H
Reaction path A								
(OOH)^q	0	2	-	-	-	-	-	0.679
	-1	1	-	-	-	-	-	0.417
	-1	3	-	-	-	-	-	0.090
Ph-CH=CH_2	0	1	1.380	-	-	-	-	-
[Ph-CH(O)-CH_2OH]^q	0	2	0.756	0.930	-0.026	0.010	0.823	-0.006
	-1	1	0.800	0.944	-0.023	-0.020	0.787	-0.022
	-1	3	0.935	0.834	-0.015	-0.048	0.699	0.010
[Ph - CH – CH_2(OH)]^q \ / O	0	2	0.817	0.674	0.001	0.669	0.001	-0.010
	-1	1	0.814	0.656	-0.020	0.685	-0.001	0.000
	-1	3	0.902	0.026	0.001	0.877	-0.002	-0.011
Reaction path B								
[CuL(OOH)]^q	0	1	-	-	-	-	-	0.720
	0	3	-	-	-	-	-	0.719
	-1	2	-	-	-	-		0.505
{[CuL(OH)](Ph-CH_2-CHO)}^{q}	0	1	0.868	-0.027	0.000	1.292	-0.012	0.001
	0	3	0.869	-0.026	0.000	1.294	-0.007	0.001
	-1	2	0.855	-0.027	0.001	1.282	-0.017	0.001
Reaction path C								
[CuL(Ph-CH=CH_2)]^q	-1	1	1.279	-	-	-	-	-
	-1	3	1.279	-	-	-	-	-
	0	2	1.379	-	-	-	-	-
{CuL[Ph-CH(OOH)-CH_2]}^{q}	0	1	0.949	0.722	-0.025	-0.025	0.000	0.530
	0	3	0.958	0.690	-0.024	-0.019	-0.001	0.529
	-1	2	0.975	0.668	-0.027	-0.043	-0.005	0.524

 doi:10.20944/preprints202506.2108.v1

2.2. Reaction Pathway B

We optimized the geometry of $[CuL]^q$ starting from its X-ray structure [13] and subsequently with added hydroperoxyl (starting from the Cu – O distance of ca 2.2 Å) in various charge and spin states (the spin multiplicity is denoted as the left superscript where necessary). After geometry optimization, the original square-planar $[CuL]^q$ complex changed its coordination to square-pyramidal only in the case of anionic doublet $^2[CuL(OOH)]^-$ (Tables S2 and S3 in Supplementary Information, Figures 4 - 5 and S5 – S6 in Supplementary Information) while its neutral analogues contain the neutral hydroperoxyl radical $(O\text{-}O_H\text{-}H_O)^0$ (see atomic charges in Table 2 and spin populations in Table 3) attached by hydrogen bonding $H_O\ldots N3$ (N3 has the highest negative charge and spin population among nitrogen atoms, see Tables 5 and 6) without any Cu-O bond (see Table 7, Figure S6 and Tables S2 – S3 in Supplementary Information). The anionic complexes $^1[CuL]^-$ and $^2[CuL(OOH)]^-$ are more stable than their neutral analogues (Tables 1 and S1 in Supplementary Information). It can be deduced that they are related by the exothermic reaction

$$^1[CuL]^- + {}^2(OOH)^0 \rightarrow {}^2[CuL(OOH)]^- \qquad (2)$$

as indicated by the reaction Gibbs energy under normal conditions $\Delta_rG_{298} = -56.37$ kJ/mol (Table S1 in Supplementary Information).

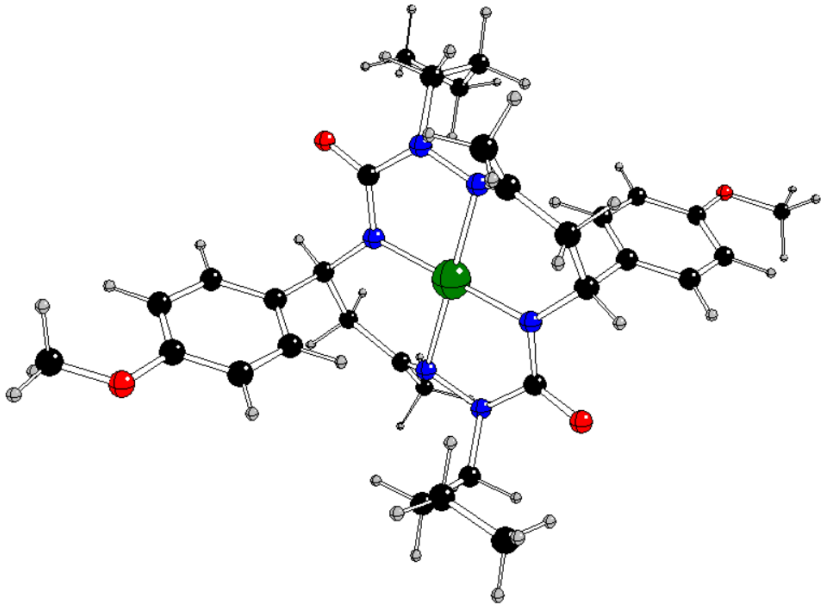

Figure 4. DFT optimized structure of $[CuL]^-$ in singlet spin state (Cu – green, C – black, N – blue, O – red, H – gray).

 doi:10.20944/preprints202506.2108.v1

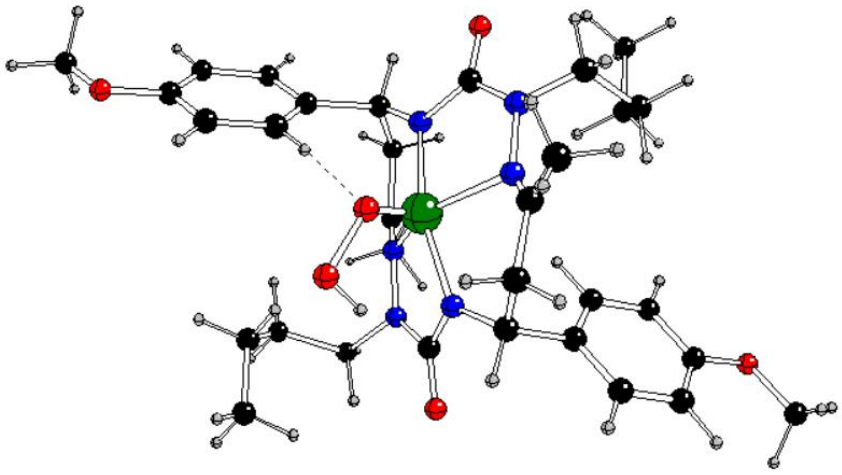

Figure 5. DFT optimized structure of $[CuL(O\text{-}O_H\text{-}H_O)]^-$ in doublet spin state (Cu – green, C – black, N – blue, O – red, H – gray).

Table 5. Natural charges of the relevant atoms in some compounds under study with charges q and spin multiplicities M_s (see Figure 1 for atom notation).

	q	M_s	Cu	N1	N3	N2
H_2L	0	1	-	-0.357(2×)	-0.680(2×)	-0.383(2×)
Reaction path B						
$[CuL]^q$	0	2	0.927	-0.339(2×)	-0.787(2×)	-0.363(2×)
	-1	1	0.603	-0.356(2×)	-0.784(2×)	-0.404(2×)
	-1	3	0.853	-0.334	-0.748	-0.373
				-0.504	-0.781	-0.366
$[CuL(OOH)]^q$	0	1	0.925	-0.348(2×)	-0.859	-0.350
					-0.793	-0.355
	0	3	0.925	-0.348(2×)	-0.859	-0.350
					-0.793	-0.355
	-1	2	0.903	-0.315	-0.777	-0.369(2×)
				-0.332	-0.750	
$\{[CuL(OH)](Ph\text{-}CH_2\text{-}CHO)\}^q$	0	1	0.923	-0.296	-0.651	-0.350
				-0.303	-0.677	-0.347
	0	3	0.955	-0.295	-0.670	-0.337
				-0.307	-0.722	-0.348
	-1	2	0.956	-0.312	-0.751	-0.376
				-0.317	-0.743	-0.356
Reaction path C						
$[CuL(Ph\text{-}CH{=}CH_2)]^q$	-1	1	0.670	-0.326	-0.785	-0.411
				-0.270	-0.782	-0.356
	-1	3	0.885	-0.377	-0.774	-0.372(2×)
				-0.396	-0.781	

 doi:10.20944/preprints202506.2108.v1

	0	2	0.928	-0.340	-0.787	-0.362(2×)
				-0.342	-0.783	
{CuL[Ph-CH(OOH)-CH_2]}^{q}	0	1	0.931	-0.340	-0.787	-0.363
				-0.342	-0.784	-0.363
	0	3	0.926	-0.341	-0.787	-0.362
				-0.341	-0.780	-0.363
	-1	2	0.848	-0.310(2×)	-0.778	-0.390
					-0.759	-0.351

Table 6. Natural spin populations of the relevant atoms in some compounds under study with charges q and spin multiplicities M_s (see Figure 1 for atom notation).

	q	M_s	Cu	N1	N3	N2
Reaction path B						
[CuL]^q	0	2	0.526	0.115(2×)	0.111(2×)	0.006(2×)
	-1	1	0.000	0.000	0.000	0.000
	-1	3	0.590	0.090	0.098	0.001
				0.345	0.115	0.006
[CuL(OOH)]^q	0	1	-0.532	-0.110(2×)	-0.111	-0.011
					-0.116	-0.006
	0	3	0.525	0.110(2×)	0.110	0.011
					0.116	0.006
	-1	2	0.575	0.054	0.106(2×)	0.002
				0.047		0.004
{[CuL(OH)](Ph-CH_2-CHO)}^{q}	0	1	0.197	0.104(2×)	-0.061	0.008
					0.022	0.003
	0	3	0.673	0.138(2×)	0.296	0.050
					0.186	0.008
	-1	2	0.610	0.059	0.109	0.000
				0.065	0.106	0.002
Reaction path C						
[CuL(Ph-CH=CH_2)]^q	-1	1	0.000	0.000	0.000	0.000
	-1	3	0.571	0.153	0.111	0.000
				0.166	0.108	0.002
	0	2	0.526	0.115(2×)	0.112	0.006(2×)
					0.110	
{CuL[Ph-CH(OOH)-CH_2]}^{q}	0	1	0.527	0.115(2×)	0.112	0.007(2×)
					0.109	
	0	3	0.527	0.115(2×)	0.111(2×)	0.007(2×)
	-1	2	0.507	0.000	0.083	-0.001
				0.023	0.087	0.002

 doi:10.20944/preprints202506.2108.v1

The spin population in ^{2}[CuL(OOH)]$^-$ is located mainly at Cu, unlike the spinless ^{1}[CuL]$^-$. Consequently, the spin transfer from neutral hydroperoxyl radical to central Cu atom can be concluded in reaction (2) which is connected with weakening of the O-O$_H$ bond (Tables 4 and 5).

Subsequent addition of neutral styrene to the hydroperoxyl group in ^{2}[CuL(OOH)]$^-$ similarly to reaction pathway A (due to sterical reasons C$_\beta$ must be close to O and C$_\alpha$ close to OH) causes hydrogen and oxygen transfers resulting to ^{2}{[CuL(OH)](Ph-CH$_2$-CHO)}$^-$ where Ph-CH$_2$-CH=O is only weakly bonded to [CuL(OH)]$^-$ (Figure 6, Tables 7 and S2 – S3 in Supplementary Information). Here, the O atom originally bonded to Cu is moved to C$_\beta$ simultaneously with H transfer from C$_\beta$ to C$_\alpha$ and Cu is bonded to O$_H$ of hydroperoxyl. It is interesting that if we remove one electron, analogous neutral complexes are obtained (Figure S7, Tables S2 – S3 in Supplementary Information) with significantly higher energies (Tables 1 and S1 in supplementary Information). Consequently, the C$_\alpha$-C$_\beta$ bonds are weakened and the double C$_\beta$=O bonds are formed (Figure 4). The strengths of Cu-O bonds are comparable with those of Cu-N1/N3 (Figure 7) and the Cu coordination is square-pyramidal (unlike

Table 7. Overlap weighted bond orders of the relevant atoms in some compounds under study with charges q and spin multiplicities M$_s$ (see Figure 1 and Table 2 for atom notation).

	q	M$_s$	Cu-N1	Cu-N3	Cu-O/O$_H$	Cu-C$_{\alpha/\beta}$
Reaction path B						
[CuL]^q	0	2	0.260(2×)	0.339(2×)	-	-
	-1	1	0.188(2×)	0.298(2×)	-	-
	-1	3	0.272	0.338	-	-
			0.357	0.346		
[CuL(OOH)]^q	0	1	0.232	0.311	0.069	-
			0.230	0.305	0.015	
	0	3	0.232	0.310	0.070	-
			0.230	0.305	0.015	
	-1	2	0.238	0.305	0.302	-
			0.215	0.313	0.023	
{[CuL(OH)](Ph-CH$_2$-CHO)}^{q}	0	1	0.293	0.384	0.000	0.000(2×)
			0.297	0.391	0.333	
	0	3	0.287	0.362	0.000	0.000(2×)
			0.295	0.386	0.333	
	-1	2	0.241	0.308	-0.001	0.004
			0.233	0.310	0.309	0.009
Reaction path C						
[CuL(Ph-CH=CH$_2$)]^q	-1	1	0.172	0.220	-	0.195
			0.132	0.240		0.240
	-1	3	0.287	0.332(2×)	-	-0.001
			0.294			0.007
	0	2	0.259(2×)	0.338(2×)	-	0.001(2×)
{CuL[Ph-CH(OOH)-CH$_2$]}^{q}	0	1	0.258(2×)	0.337	0.000(2×)	0.000(2×)
				0.333		
	0	3	0.258	0.337	0.000(2×)	0.000(2×)
			0.260	0.339		

 doi:10.20944/preprints202506.2108.v1

-1	2	0.161	0.277	0.010	0.052
		0.178	0.262	0.003	0.324

square-planar $[CuL]^q$, see Tables S2-S3 in Supplementary Information). Non-vanishing spin populations in the compounds within this reaction pathway can be at Cu, N1, N3 and hydro(perox)yl oxygen atoms (Tables 3 and 6). Cu in $^1[CuL]^-$ has a less positive charge and no spin population, which implies the oxidation state of Cu(I) (Tables 2 and 5). More positive Cu charges and nonzero spin populations in other compounds of this reaction pathway correspond to the oxidation state Cu(II).

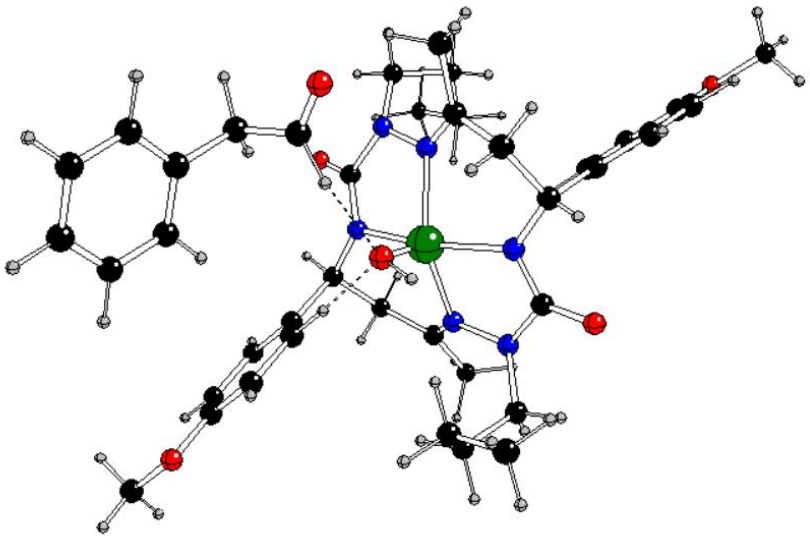

Figure 6. DFT optimized structure of $\{[CuL(O_H\text{-}H_O)](Ph\text{-}C_\alpha H_2\text{-}C_\beta HO)\}^-$ in doublet spin state (Cu – green, C – black, N – blue, O – red, H – gray).

The most probable styrene oxidation step can be described by the exothermic reaction

$$^2[CuL(OOH)]^- + Ph\text{-}CH{=}CH_2 \rightarrow {}^2\{[CuL(OH)](Ph\text{-}CH_2\text{-}CHO)\}^- \quad (3)$$

as indicated by the reaction Gibbs energy under normal conditions Δ_rG_{298} =-266.67 kJ/mol (Table S1 in Supplementary Information).

2.3. Reaction Pathway C

We optimized the structures of $[CuL(Ph\text{-}CH{=}CH_2)]^q$ starting from the optimized structures of $[CuL]^q$ with added neutral styrene in the form of a π-complex with Cu-$C_{\alpha/\beta}$ distances of ca 2.4 Å. Only the optimized structure of $^1[CuL(Ph\text{-}CH{=}CH_2)]^-$ preserved the original form of a π-complex where the Cu- $C_{\alpha/\beta}$ bond lengths are comparable with the Cu-N1/N3 ones and the square-planar Cu coordination lost its planarity (Figure 7, Tables S2 – S3 in supplementary Information). Its $^1[CuL(Ph\text{-}CH{=}CH_2)]^0$ and $^3[CuL(Ph\text{-}CH{=}CH_2)]^-$ analogues with separated square-planar $[CuL]^q$ and neutral Ph-CH=CH_2 components are energetically higher (Tables 1, S1 – S3, and Figure S8 in Supplementary Information).

 doi:10.20944/preprints202506.2108.v1

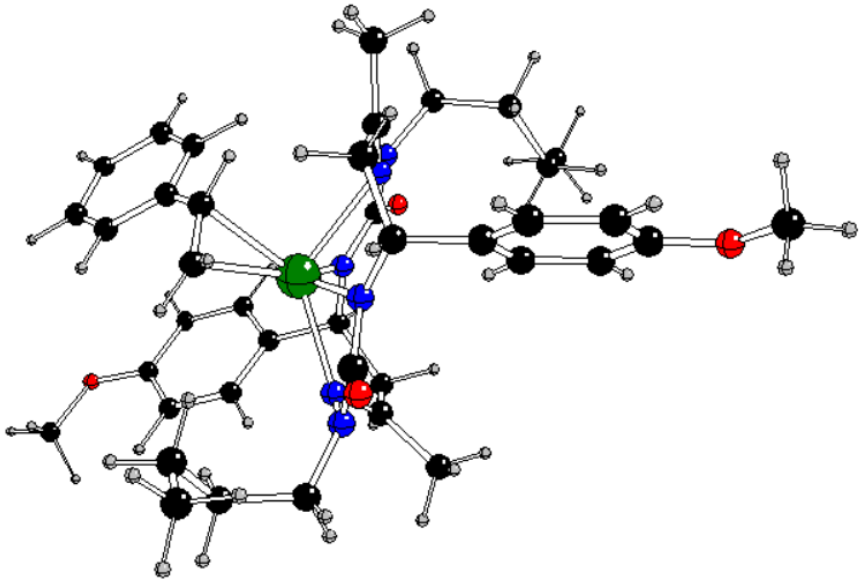

Figure 7. DFT optimized structure of $[CuL(Ph\text{-}C_{\alpha}H{=}C_{\beta}H_2)]^-$ in singlet spin state (Cu – green, C – black, N – blue, O – red, H – gray).

The lower charge and absence of spin at Cu in $^1[CuL(Ph\text{-}CH{=}CH_2)]^-$ indicates the formal oxidation state Cu(I) unlike the Cu(II) one in $[CuL]^q$, $^1[CuL(Ph\text{-}CH{=}CH_2)]^0$ and $^3[CuL(Ph\text{-}CH{=}CH_2)]^-$ (Tables 5 – 6). The Cu-N1/N3 bonds in $^1[CuL(Ph\text{-}CH{=}CH_2)]^-$ are weaker than in $[CuL]^q$ and comparable with the Cu-$C_{\alpha/\beta}$ ones (Table 7). The $C_{\alpha}{=}C_{\beta}$ bond strength is equal to that of free styrene (Table 4).

According to our results, the only stable π-complex can be obtained by the non-radical endothermic reaction

$$^1[CuL]^- + Ph\text{-}CH{=}CH_2 \rightarrow {}^1[CuL(Ph\text{-}CH{=}CH_2)]^- \qquad (4)$$

as indicated by the reaction Gibbs energy under normal conditions Δ_rG_{298} = +91.95 kJ/mol (Table S1 in Supplementary Information).

The addition of the hydroperoxyl radical to $^1[CuL(Ph\text{-}CH{=}CH_2)]^-$ leads to $^2\{CuL[Ph\text{-}CH(OOH)\text{-}CH_2]\}^-$ (analogously to the reaction pathway A) with a split Cu-C_{α} bond and hydroperoxyl bonding to the C_{α} site (Figure 8, Tables S2-S3 in Supplementary Information). Subsequently, the spin density is moved from hydroperoxyl to Cu with a higher positive charge corresponding to the real oxidation state instead of Cu(I) in $^1[CuL(Ph\text{-}CH{=}CH_2)]^-$ (Tables 2, 3, 5, and 6). The Cu-N1/N3 bonds are weaker than the Cu-C_{β} one in $^1[CuL(Ph\text{-}CH{=}CH_2)]^-$ (Table 7).

 doi:10.20944/preprints202506.2108.v1

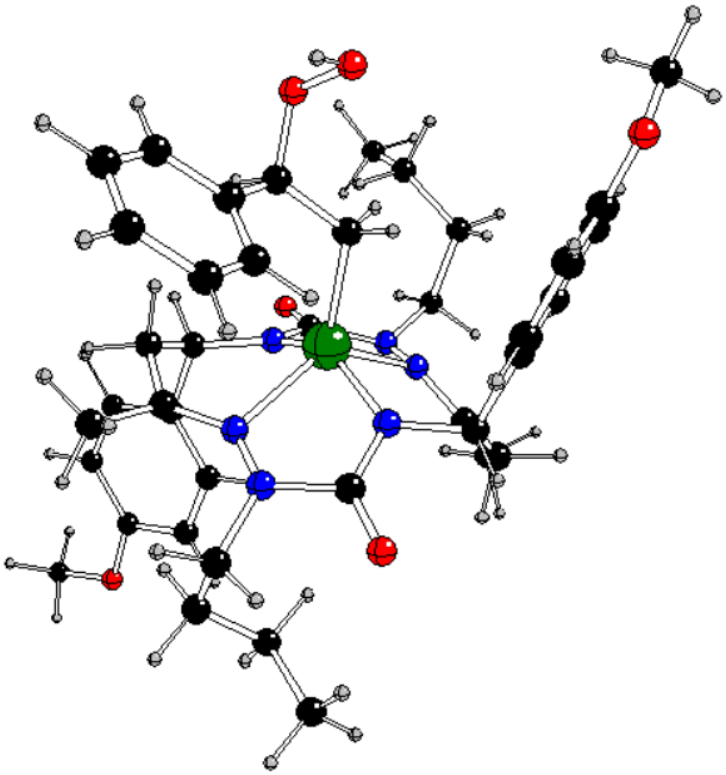

Figure 8. DFT optimized structure of {CuL[Ph-C_αH(O-O_H-H_O)-$C_\beta H_2$]}$^-$ in doublet spin state (Cu – green, C – black, N – blue, O – red, H – gray).

An electron removal from ^{1}[CuL(Ph-CH=CH_2)]$^-$ should correspond to the formal oxidation state Cu(II) but it causes the Ph-CH(OOH)-CH_2 split from the [CuL]^0 unit (Tables S2-S3 and Figure S9 in Supplementary Information) with higher energies (Tables 1 and S1 in Supplementary Information). Based on charges and spin populations (Tables 2, 3, 5 and 6), the real Cu(II) oxidation state is preserved in neutral [CuL(Ph-CH=CH_2)]^0 complexes and the spin density is moved from hydroperoxyl to N1 and N3 atoms.

Our results show that the most advantageous hydroperoxyl addition to the above mentioned π-complex can be described by the endothermic reaction

$$^1[CuL(Ph\text{-}CH{=}CH_2)]^- + {}^2(OOH)^0 \rightarrow {}^2\{CuL[Ph\text{-}CH(OOH)\text{-}CH_2]\}^- \qquad (5)$$

as indicated by the reaction Gibbs energy under normal conditions $\Delta_r G_{298}$ = -35.92 kJ/mol (Table S1 in Supplementary Information).

3. Method

Geometry optimization of the systems under study was performed using B3LYP hybrid functional [14] and 6-311+G* basis sets from the Gaussian library [15]. The optimized structures were tested on the absence of imaginary vibrations using vibrational analysis. Singlet spin states in Cu complexes were treated using an unrestricted formalism and their energies related to triplet spin states were corrected as follows ('broken symmetry' treatment, BS) [16].

$$E_S - E_T = \frac{\langle S^2\rangle_T (E_{BS} - E_T)}{\langle S^2\rangle_T - \langle S^2\rangle_{BS}} \qquad (6)$$

E_S, E_T and E_{BS} are singlet, triplet, and 'broken symmetry' (unrestricted singlet) energies, respectively. $\langle S^2\rangle_T$ and $\langle S^2\rangle_{BS}$ are triplet and 'broken symmetry' values of spin squares, respectively. Atomic

 doi:10.20944/preprints202506.2108.v1

charges, spin populations, and overlap weighted bond orders were evaluated in terms of natural population analysis [17,18]. All quantum-chemical calculations were performed using Gaussian16 software [15]. The MOLDRAW software was used for geometry manipulation and visualization purposes [20].

4. Conclusions

Using quantum-chemical treatment, relevant intermediates in various charge and spin states of three reaction pathways of styrene oxidation by hydroperoxyl were investigated. The reaction pathway A without any catalyst probably proceeds by non-radical mechanism when neutral styrene is attacked by a hydroperoxyl anion and ^{1}[Ph-CH(O)-CH$_2$OH]$^-$ is formed (Figure 2). The alternative formation of epoxide (Figure 3) is energetically less advantageous.

The alternative reaction pathways B and C are based on the [CuL]^q catalyst (Figure 1), most probably its anionic form in the singlet spin state corresponding to the formal oxidation state Cu(I). Within the reaction pathway B the neutral hydroperoxyl radical is bonded to Cu to form ^{2}[CuL(OOH)]$^-$ (Figure 4) which is unstable in other charge and spin states. The spin density is moved to Cu, which corresponds to the real oxidation state of Cu(II). Subsequent addition of neutral styrene results in ^{2}{[CuL(OH)](Ph-CH$_2$-CHO)}$^-$ formation after significant O and H atoms rearrangements which contains only weakly bonded ^{2}[CuL(OH)]$^-$ and Ph-CH$_2$-CH=O units. This reaction pathway seems to be realistic, but in future studies we must solve the Cu-OH split (probably by reaction with hydroperoxyl as in [4,5]) and the formation of benzaldehyde (by interaction with hydroperoxyl [4] or with ^{2}[CuL(OH)]$^-$ [3,7]).

The reaction pathway C starts with the initial non-radical formation of the π-complex ^{1}[CuL(Ph-CH=CH$_2$)]$^-$ (Figure 7) with the oxidation state of Cu(I) according to Eq. (4) but this reaction is problematic because of its endothermic character. However, its analogues in other charge and spin states do not allow for such a π-complex formation. Subsequent addition of a hydroperoxyl radical leads to ^{2}{CuL[Ph-CH(OOH)-CH$_2$]}$^-$ (Figure 8) with Cu-C$_\beta$ bonding. Its oxidation leads to Ph-CH(OOH)-CH$_2$ separation.

Our study explains why reaction pathway B of the catalytic oxidation of styrene by hydroperoxylating a bis-semicarbazide hexaazamacrocyclic Cu complex is preferred. Our future studies will provide additional details of its reaction mechanism, including solvent effects.

Supplementary Materials: The following supporting information can be downloaded at the website of this paper posted on Preprints.org, Table S1: DFT energies, E_{DFT}, and Gibbs energies at 298 K, G_{298}, of the compounds under study with charges q, spin multiplicities M_s, and spin squares $\langle S^2 \rangle$; Table S2: Selected bond lengths (in Å) between relevant atoms in the compounds under study with charges q and spin multiplicities M_s; Table S3: Selected bond angles (in degrees) in the compounds under study with charges q and spin multiplicities M_s; Figure S1: X-ray structure of H$_2$L with atom-labelling scheme and thermal ellipsoids drawn at 20% probability level; Figures S2 – S9: DFT optimized structures of the possible reaction intermediates in various charge q and spin states M_s.

Funding: Slovak Grant Agency VEGA (contract No. 1/0175/23) is acknowledged for financial support.

Data Availability Statement: Data is contained within the article or supplementary material.

Acknowledgments: We thank the HPC center at the Slovak University of Technology in Bratislava, which is a part of the Slovak Infrastructure of High-Performance Computing (SIVVP Project, ITMS code 26230120002, funded by the European Region Development Funds), for computing facilities. .

Conflicts of Interest: The author declares no conflicts of interest.

References

1. Andrade, M.A.; Martins, L.M.D.R.S. Selective Styrene Oxidation to Benzaldehyde over Recently Developed Heterogeneous Catalysts. *Molecules* **2021**, *26*, 1680 and the references cited in.

 doi:10.20944/preprints202506.2108.v1

2. *Keith, J.A.; P. M. Henry, P.M. The Mechanism of the Wacker Reaction: A Tale of Two Hydroxypalladations. Angew. Chem. Int. Ed. 2009, 48,* 9038–*9049.*
3. Zhou. Sh.; Chen, X.; Qia, Ch. Quantum chemical modeling of the epoxidation with hydrogen peroxide catalyzed by Mn(III): Mechanistic insight. *Chem. Phys. Let.* **2010,** *488*, 44–49.
4. Lashanizadegan, M.; Alavijeh, R.K.; Anafcheh, M. Facile synthesis of Co(II) and Cu(II) complexes of 2-hydroxybenzophenone: An efficient catalyst for oxidation of olefins and DFT study. *J. Mol. Struct.* **2017,** *1146*, 450-457.
5. Lashanizadegan, M.; Ashari, H.A.; Sarkheil, M.; Anafcheh, M.; Jahangiry, S. New Cu(II), Co(II) and Ni(II) azo-Schiff base complexes: Synthesis, characterization, catalytic oxidation of alkenes and DFT study. *Polyhedron* **2021**, *200,* 115148.
6. Lashanizadegan, M.; Habibi, N.; Mirzazadeh, H.; Ghiasi, M. Immobilized magnetic copper hydrazine complexes for oxidation of styrene to benzaldehyde by tert-butylhydroxyperoxide: an experimental and theoretical approach. *React. Kinet., Mechan. Catal.* **2022**, *135*, 3223–3242.
7. Yang, R.A.; Sarazen, M.L. Mechanistic Impacts of Metal Site and Solvent Identities for Alkene Oxidation over Carboxylate Fe and Cr Metal–Organic Frameworks. *ACS Catal.* **2022**, *12*, 14476−14491.
8. Wu, Y.; Kang, J.; Gao, W.; Bi, M.; Yang, D.; Ji, R.; Meng, Q.; Ma, C. A DFT and kinetic study: Is it possible to prepare epoxides without catalysts using the in-situ generated peroxy radicals or peroxides by one-step method? *J. Comput. Chem.* **2023**, *44*, 1917–1927.
9. Abuhafez, N.; Ehlers, A.W; de Bruin, B.; Gramage-Doria, R. Markovnikov-Selective Cobalt-Catalyzed Wacker-Type Oxidation of Styrenes into Ketones under Ambient Conditions Enabled by Hydrogen Bonding. *Angew. Chem. Int. Ed.* **2024,** *63,* e202316825.
10. Vala, G.; Jadeja, R.N.; Patel, A.; Choquesillo-Lazarte, D. Development of novel heterogeneous cobalt acylpyrazolone catalyst: Synthesis, characterization and selective oxidation of styrene to benzaldehyde. *Inorg. Chim. Acta* **2024,** *563*, 121925.
11. Razmara, Z.; Necas, M.; Karimi , P. Oxidation of styrene by Mn (II)-pyridine-2,6-dicarboxylate complex: Synthesis, X-ray structure and DFT studies. *J. Mol. Struct.* **2025,** *1330,* 141440.
12. Sayeh, K.; Louroubi, A.; Abdallah, N.; Fkhar, L., Aflak, N.; Bahsis, L.; Hasnaoui, A.; Ali, M.A.; El Firdoussi, L. Elaboration and characterization of Zn1−xCoxFe2O4 spinel ferrites magnetic material: application as heterogeneous catalysts in styrene oxidation. *React. Kinet., Mechan. Catal.* **2025**, *138*, 911–927.
13. Dobrov, A.; Fesenko, A.; Yankov, A.; Stepanenko, I.; Darvasiova, D.; Breza, M.; Rapta, P.; Martins, L.M.D.R.S.; Pombeiro, A.J.L.; Shutalev, A.; Arion, V.B. Nickel(II), Copper(II) and Palladium(II) Complexes with Bis-Semicarbazide Hexaazamacrocycles: Redox-Noninnocent Behavior and Catalytic Activity in Oxidation and C−C Coupling Reactions. *Inorg. Chem.* **2020,** *59,* 10650−10664.
14. Becke, A. D. Density-functional Thermochemistry. III. The Role of Exact Exchange. *J. Chem. Phys.* **1993,** *98*, 5648−5652.
15. Frisch, M. J.; Trucks, G. W.; Schlegel, H. B.; Scuseria, G. E.; Robb, M. A.; Cheeseman, J. R.; Scalmani, G.; Barone, V.; Petersson, G. A.; Nakatsuji, H.; Li, X.; Caricato, M.; Marenich, A. V.; Bloino, J.; Janesko, B. G.; Gomperts, R.; Mennucci, B.; Hratchian, H. P.; Ortiz, J. V.; Izmaylov, A. F.; Sonnenberg, J. L.; Williams-Young, D.; Ding, F.; Lipparini, F.; Egidi, F.; Goings, J.; Peng, B.; Petrone, A.; Henderson, T.; Ranasinghe, D.; Zakrzewski, V. G.; Gao, J.; Rega, N.; Zheng, G.; Liang, W.; Hada, M.; Ehara, M.; Toyota, K.; Fukuda, R.; Hasegawa, J.; Ishida, M.; Nakajima, T.; Honda, Y.; Kitao, O.; Nakai, H.; Vreven, T.; Throssell, K.; Montgomery, J. A., Jr.; Peralta, J. E.; Ogliaro, F.; Bearpark, M. J.; Heyd, J. J.; Brothers, E. N.; Kudin, K. N.; Staroverov, V. N.; Keith, T. A.; Kobayashi, R.; Normand, J.; Raghavachari, K.; Rendell, A. P.; Burant, J. C.; Iyengar, S. S.; Tomasi, J.; Cossi, M.; Millam, J. M.; Klene, M.; Adamo, C.; Cammi, R.; Ochterski, J. W.; Martin, R. L.; Morokuma, K.; Farkas, O.; Foresman, J. B.; Fox, D. J. *Gaussian 16, Rev. C.01*; Gaussian, Inc.: Wallingford, CT, **2016.**
16. Malrieu, J.-P.; Trinquier, G. A Recipe for Geometry Optimization of Diradicalar Singlet States from Broken-Symmetry Calculations, *J. Phys. Chem. A* **2012**, *116*, 8226−8237.
17. Foster, J. P.; Weinhold, F. Natural Hybrid Orbitals. *J. Am. Chem. Soc.* **1980**, *102*, 7211−7218.
18. Reed, A. E.; Curtiss, L. A.; Weinhold, F. Intermolecular Interactions from a Natural Bond Orbital, Donor-Acceptor Viewpoint. *Chem. Rev.* **1988,** *88*, 899−926.

 doi:10.20944/preprints202506.2108.v1

19. Carpenter, J. E.; Weinhold, F. Analysis of the Geometry of the Hydroxymethyl Radical by the "Different Hybrids for Different Spins" Natural Bond Orbital Procedure. *J. Mol. Struct.: THEOCHEM* **1988**, *169*, 41−62.
20. Ugliengo, P. MOLDRAW: A Program to Display and Manipulate Molecular and Crystal Structures, University Torino, Torino, **2012**. Available online: https://moldraw.software.informer.com (accessed on 9 September 2019).